IOPscience iopscience.iop.org

Home Search Collections Journals About Contact us My IOPscience

Density limit studies in the tokamak and the reversed-field pinch

This content has been downloaded from IOPscience. Please scroll down to see the full text.

2015 Nucl. Fusion 55 043007

(http://iopscience.iop.org/0029-5515/55/4/043007)

View the table of contents for this issue, or go to the journal homepage for more

Download details:
This content was downloaded by: gspizzo
IP Address: 150.178.3.9
This content was downloaded on 19/03/2015 at 07:56

Please note that terms and conditions apply.

IOP Publishing | International Atomic Energy Agency Nuclear Fusion
Nucl. Fusion **55** (2015) 043007 (10pp) doi:10.1088/0029-5515/55/4/043007

Density limit studies in the tokamak and the reversed-field pinch

G. Spizzo[1], G. Pucella[2], O. Tudisco[2], M. Zuin[1], M. Agostini[1], E. Alessi[3], F. Auriemma[1], W. Bin[3], P. Buratti[2], L. Carraro[1], R. Cavazzana[1], G. Ciaccio[1], G. De Masi[1], B. Esposito[2], C. Galperti[3], S. Garavaglia[3], G. Granucci[3], M. Marinucci[2], L. Marrelli[1], E. Martines[1], C. Mazzotta[2], D. Minelli[3], A. Moro[3], M.E. Puiatti[1], P. Scarin[1], C. Sozzi[3], M. Spolaore[1], O. Schmitz[4], N. Vianello[1] and R.B. White[5]

[1] Consorzio RFX, Padova, Italy
[2] ENEA, Centro Ricerche di Frascati, Italy
[3] IFP-CNR, Via R. Cozzi 53, 20125 Milano, Italy
[4] Department of Engineering Physics, University of Wisconsin -Madison, Madison, WI, USA
[5] Plasma Physics Laboratory, Princeton University, P.O. Box 451, Princeton, NJ 08543, USA

E-mail: gianluca.spizzo@igi.cnr.it

Received 28 November 2014, revised 30 January 2015
Accepted for publication 18 February 2015
Published 18 March 2015

Abstract

The ITER scenarios and the project of DEMO involve stable operation above the Greenwald density, which justifies efforts to understand and overcome the density limit, this last observed as a disruptive termination of tokamak discharges and a thermal crash (with no disruption) of stellarator and reversed-field pinch (RFP) ones. Both in the tokamak and the RFP, new findings show that the high density limit is not governed by a unique, theoretically well-determined physical phenomenon, but by a combination of complex mechanisms involving two-fluid effects, electrostatic plasma response to magnetic islands and plasma–wall interaction. In this paper we will show new evidence challenging the traditional picture of the 'Greenwald limit', in particular with reference to the role of thermal instabilities and the edge radial electric field E^r in the development of this limit.

Keywords: theory, design, and computerized simulation, particle orbits, two-fluid and multi-fluid plasmas, particle orbit and trajectory, plasma–material interactions, boundary layer effects

(Some figures may appear in colour only in the online journal)

1. Introduction

The density limit was described in the 1980s by Greenwald [1], by re-expressing the Hugill limit [2] in terms of the parameter $n_G = I/\pi a^2$ ('Greenwald' density), which was to be widely used to describe the phenomenology of the high density in tokamaks and reversed-field pinches (RFP). Anyway, scalings of a critical density for the appearance of strong $m = 2$ activity lead to a dependence with the magnitude of B, as shown in the 1980s by Granetz [3]. In the stellarator community it is common to find a milder scaling with the magnetic field, plus a scaling with the heating power, namely, the Sudo limit [4] with $n_S = 0.25 \cdot (\frac{PB}{a^2 R})^{0.5}$. Both in the tokamak and the RFP, new findings show that the high density limit, which often disrupts tokamak discharges and slowly terminates RFP ones, is not governed by the unique n_G parameter, but by a combination of complex mechanisms involving two-fluid effects: namely, the electrostatic plasma response to magnetic islands and related plasma–wall interaction (PWI), and input power, as in the Sudo scaling. This is quite relevant for the fusion research, since ITER scenarios and the project of DEMO [5] both involve stable operation above the Greenwald density, $\langle n_e \rangle \gtrsim 1.2\, n_G$, but most tokamaks run within $\langle n_e \rangle \lesssim 0.6\, n_G$, or even less, to avoid H–L back-transition and detachment [6–8]. Moreover, in tokamaks and RFPs, edge and scrape-off layer (SOL) profiles, the radial electric field E^r along with the turbulence, all change at a reduced Greenwald fraction $\langle n_e \rangle \approx 0.35\, n_G$ [9–13]. This justifies the effort to put into relationship properties of the edge/SOL at high collisionality, and the density limit, in order to understand and overcome it.

In this paper we will investigate results of the L-mode density limit in the FTU tokamak, in combination with results of the density limit in the RFX RFP, both circular, ohmic machines covering together a wide range of toroidal

 © 2015 EURATOM Printed in the UK

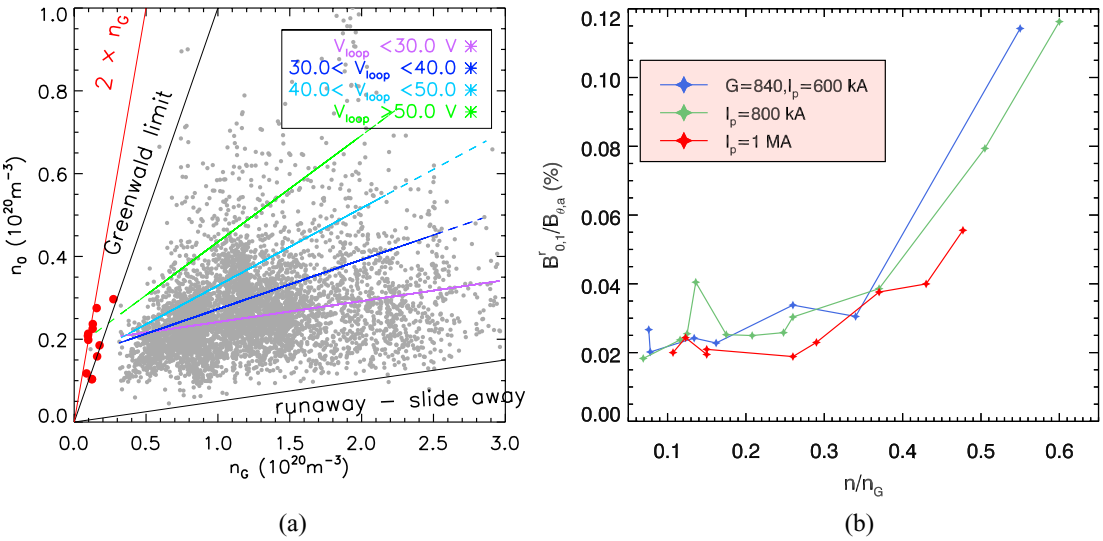

Figure 1. Phenomenology of the density limit in the RFP: (*a*) data points in the Greenwald plane: straight lines are interpolation of points grouped according to intervals of loop voltage. Red points are discharges at low current and $n_0 \sim 2n_G$; (*b*) $m = 0$ mode amplitude, B^r component at $r = a$, normalized to the equilibrium poloidal field $B_{\theta,a}$, as a function of n/n_G, three values of plasma current.

magnetic field values. The goal is to add relevant information in the quest for a common physical mechanism which, if properly understood, could in principle be extended to other configurations, namely, the stellarator and diverted, auxiliary heated tokamaks. Particular emphasis will be given to the properties of the flow in the edge/SOL region, and to the role of thermal instabilities in setting the environment for the development of the limit. A model developed to explain the limit in the RFP will be presented, it shows the importance of convective cells dragging density in the stochastic edge of the RFP. This model will be compared to FTU, in particular regarding the role of the 2/1 mode in the disruptions that terminate the discharge at high density. The paper is organized as follows: in section 2 the phenomenology of the density limit, and the parameters that govern it, are presented; in section 3 the radial instability is discussed, together with the model of the convective cell in the RFP edge; in section 4 the role of the MHD tearing modes (TMs) in both RFX and FTU is shown. Finally, in section 5 we draw our conclusions.

2. Density limit phenomenology and scalings

2.1. Density limit phenomenology in the RFX RFP

In the RFX RFP [14], data points in the plane (n_G, n_0), with n_0 the central electron density, seem to follow a Hugill–Greenwald scaling, with scarce data points for $n_0 > n_G$, as published several times in the past [15–21], but a real disruptive limit when approaching n_G has never been found [18, 20]. This can be highlighted by grouping data in classes, according to the value of the toroidal loop voltage, as shown in figure 1(*a*). The straight lines in the plot correspond almost exactly to curves at constant V_{loop}: moreover, it is evident that the larger the V_{loop}, the steeper the slope of n_0 versus n_G. This means that, with enough loop voltage, in the RFP it is possible to get $n_0 = n_G$ with no disruption. This can be done at low current, since the ohmic input power is low despite the high voltage, as shown in figure 1(*a*) as red points: the Greenwald limit is exceeded by a factor ∼2. Moreover, a linear regression of V_{loop} as a function of n_0/n_G in the RFX database, represented by the grey points of figure 1(*a*), gives as a result $V \approx 12 + 60\, n_0/n_G$. The same linear law was seen to hold between the effective charge Z_{eff} and V_{loop} in the old RFX, with a bias loop voltage of $V_{dyn} \sim 17$ V, which was interpreted as a minimum value to sustain the RFP dynamo [22]. This means that the limit has a radiative nature, with a difficulty in performing high current and high density discharges, that require an exceedingly large input power. Nevertheless, no clear disruption is seen, so that it is impossible in the RFP to define a 'critical' density, e.g. on the basis of a soft x-ray crash and associated loss of the plasma thermal content. This is a clear advantage of the RFP configuration over the tokamak, being summarized in the empirical, linear law

$$V \approx 12 + 60\,\frac{n_0}{n_G} = V_{dyn} + V_G \frac{n_0}{n_G}, \qquad (1)$$

where $V_{dyn} = 12$ V is the bias dynamo voltage, and $V_G = 60$ V is the voltage required to reach the Greenwald limit. Since the RFP heating is ohmic, multiplying equation (1) by n_G, we get $(V - V_{dyn})\, I_p = V_G \pi a^2\, n_0$, which is a linear dependence of the central density on heating power (input power minus the dynamo term). This dependence has indeed been reported for RFX [23]: with larger input power, larger densities can be accessed. This is a result reminiscent of the Sudo scaling, and it has been shown in the past also in the TEXTOR tokamak [24]. In the same paper [23], it was reported that, with lithization, the power required to get to the same density is half as much as in standard RFX discharges. According to equation (1), this means that also V_G can be greatly reduced with wall conditioning. Another means of increasing central density without impacting too much on the loop voltage is pellet injection, as demonstrated in the Madison Symmetric Torus (MST) RFP where n_G can be easily exceeded with this technique [25]. In MST too, no disruption is seen crossing the Greenwald limit.

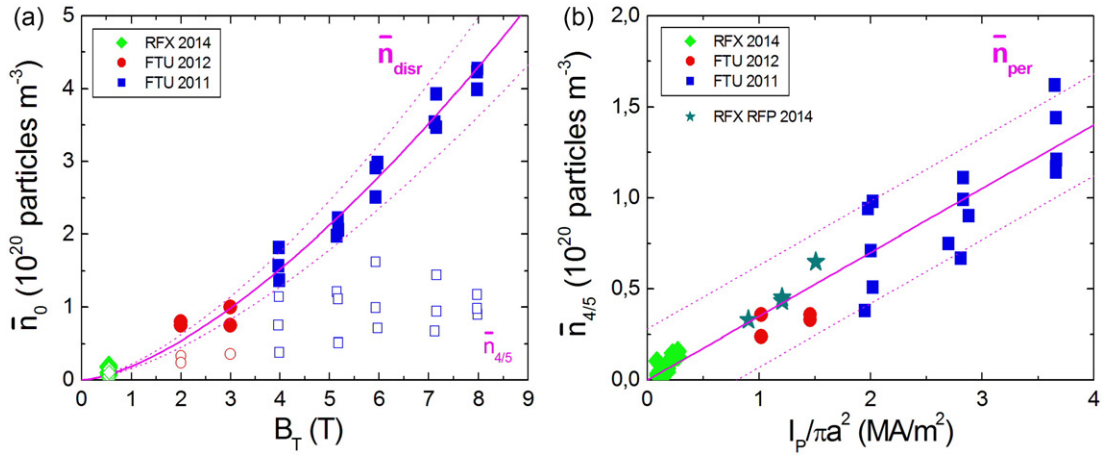

Figure 2. Phenomenology of the density limit in the FTU tokamak: (a) full symbols are the central ($r/a = 0$) line-averaged density at the disruption $\bar{n}_{\rm disr}$ versus the toroidal magnetic field. Ranges of current and q: $I_{\rm p} = 250 \div 900$ kA, $q_a = 2.3 \div 8.5$. With open symbols, the peripheral ($r/a = 0.8$) line-averaged density is over-plotted as a function of $B_{\rm T}$. At the disruption, the edge density does not follow a scaling with the magnetic field, contrary to the core density. (b) Peripheral line-averaged density $\bar{n}_{\rm per}$ at the disruption versus Greenwald. Green points (in both panels) are data from RFX, run in tokamak configuration, ranges of current and q: $I_{\rm p} = 60 \div 180$ kA, $q_a = 1.9 \div 4.6$. Light blue stars are the critical density for the onset of a large $0/1$ mode in RFX operated as RFP. This MHD limit for the RFP coincides with the FTU disruptive limit for the edge density.

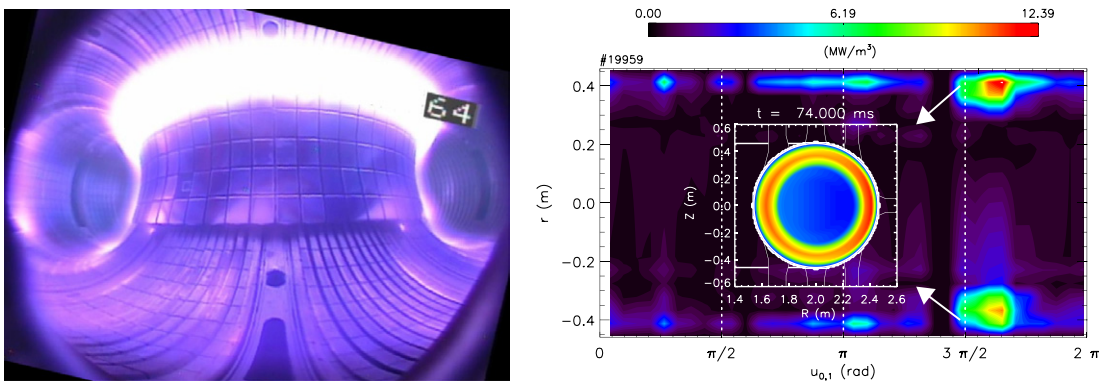

(a) (b)

Figure 3. (a) Camera image of the MARFE in FTU (visible, mainly H $_\alpha$ emission); (b) equatorial map of total emission (toroidal angle on the x-axis), showing the poloidal MARFE of RFX as two bright, toroidally localized spots: in the inset, a tomographic map on a poloidal section, at the toroidal location of the spots.

A clear threshold with a critical density can be defined instead on a MHD basis, as done by Granetz on Alcator [3]. In fact, by increasing density, in the RFP we destabilize the $m/n = 0/1$ mode, which is responsible for the development of a MARFE, as it will be shown in section 3. In this sense, the RFP density limit is more a non-disruptive, MHD limit: in fact, it has already been published that the $m = 0, n < 7$ modes increase sharply as a function of $n_0/n_{\rm G}$ (at constant current) [21], and that this is a pre-requisite for the development of the MARFE [26]. In figure 1(b) we report results from recent experiments (April 2014), where we tried to stabilize the $0/1$ mode with the feedback controlled, 192 active coil system of RFX [27]: indeed, the normalized, perturbed radial field at $r = a$, $B^r_{0,1}/B_{\theta,a}$ remains low, until a threshold $n_0 \sim 0.35\, n_{\rm G}$ is reached, then it shows an explosive behaviour. The threshold follows a Greenwald-like scaling, which recently has been put into relationship with the Prandtl number [28] which in visco-resistive MHD simulations governs the stability of the $m = 0$ modes [29]. This result is confirmed in a range of plasma currents $I_{\rm p} = 0.6 \div 1$ MA with shallow reversal, $q_a = -0.015$ (corresponding to a reversal parameter $F = B_{\varphi,a}/\langle B_\varphi \rangle = -0.08$).

2.2. Density limit phenomenology in the FTU tokamak

Let us consider now the FTU tokamak, which is a circular tokamak running in L-mode [30]. The edge density ($r/a = 0.8$) at the disruption is shown in figure 2(b): it follows a reduced, Greenwald scaling of the form

$$n_{\rm edge} \sim 0.35\, n_{\rm G}. \qquad (2)$$

It is striking that the threshold of equation (2) coincides with the RFP MHD limit, taking into account that density profiles in the RFP are usually flat at intermediate–low density, with $n_0 \sim n_{\rm edge}$: this is shown in figure 2(b) as light blue stars. Contrary to the RFP, in FTU the maximum achievable central density essentially depends on the toroidal magnetic field only [31], with a Granetz-like scaling $n_0 = 0.19\, B^{1.5}$ [units

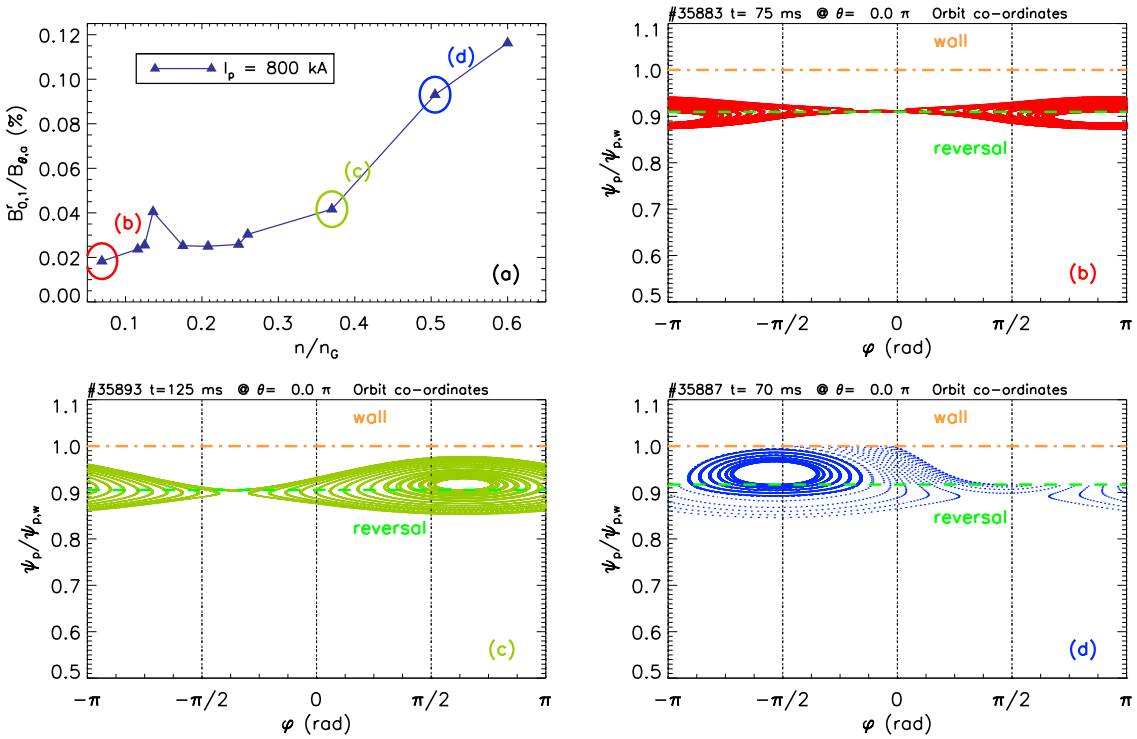

Figure 4. Trigger of the MARFE in the RFX RFP. (*a*) Density scan of the $m = 0$ mode amplitude at plasma current $I_p = 800\,\mathrm{kA}$; (*b*)–(*d*), Poincaré plots of the 0/1 island, toroidal angle on x-axis, normalized flux coordinate on y-axis, for three discharges marked as circles in frame (*a*). The critical size of the island is reached when the flux surfaces intercept the first wall.

$10^{20}\,\mathrm{m}^{-3}$ and T, see figure 2(*a*)]. This behaviour can be explained in terms of density peaking, since the edge density (open symbols in figure 2(*a*)) does not depend on B, as shown in equation (2). In fact, in FTU with a stronger B field (and the same current level) disruption happens later in the discharge, and larger core densities can be accessed, i.e. with larger peaking. This is shown in figure 6 in [32]. The behaviour of core and edge density *at the disruption* can be summarized as a scaling $n_0/n_{\mathrm{edge}} \propto q_a$, shown in figure 8 of [32]. A similar scaling $|\nabla n|/n \propto \nabla q/q$ has been put into relationship with the theory of the 'curvature pinch' [33] in a smaller database of auxiliary heated discharges [34] (not considered in this paper), but no clear theoretical answer to the peaking phenomenon has yet been given in FTU. Combining the empirical law $n_0/n_{\mathrm{edge}} \propto q_a$ with the Greenwald edge scaling, it is obtained $n_0 \sim 0.7\,B/\mu_0 R$. Curiously, this is the Murakami parameter [35] which was used in the early research on the density limit. In other words, in experiment, the edge density is set by the plasma current: $n_{\mathrm{edge}} \sim 0.35\,n_{\mathrm{G}} = 0.35\,I_{\mathrm{p}}/\pi a^2$. For a given n_{edge}, the maximum n_0 prior to disruption is determined by the profile peaking, namely, by the value of q_a. For a given plasma current, this means that the maximum central density n_0 is determined by B. Conversely, the smaller B, the smaller n_0 and the flatter the density profile: in these cases, n_0 follows also a Greenwald scaling. This is the case of the RFX device (green points in figure 2), which can be operated also as a low-B tokamak with a flexible feedback control system [36]. In the RFX tokamak, n_0 follows the scaling with the magnetic field, but also a Greenwald scaling, since density profiles are essentially flat: as a consequence, full and open symbols in figure 2(*a*) collapse one over the other.

Historically, the dependence on $|\vec{B}|$ was lost in the original 1988 paper by Greenwald [1]: in the Hugill plane [2], which displays the inverse safety factor versus the Murakami parameter [35], a straight line corresponds to a critical density n_{c} such that

$$\frac{1}{q_a} \propto n_{\mathrm{c}} \frac{\mu_0 R}{2B} \rightarrow n_{\mathrm{c}} = \frac{I_p}{\pi a^2}, \tag{3}$$

which is the definition of n_{G}. In this way the dependence on $|\vec{B}|$ is completely lost. On the contrary, from the point of view of basic plasma physics, recently B was found to be the single parameter limiting the maximum achievable core density in laboratory and astrophysical plasmas [37]. The results from FTU [31, 32] confirm and strongly re-propose the B-limit for the central density, plus a reduced-Greenwald limit (equation (2)) for the edge density. As a matter of fact, the only machines operating with a central density $n_0 \approx n_{\mathrm{G}}$ are those possessing the strongest fields, namely, FTU and ALCATOR. This could be a concern for DEMO and/or ITER, since with a lower range of B a lower density peaking can be obtained, although transient density peaking can be induced via pellet injection and/or NBI [25, 38, 39]. Therefore, density in ITER and DEMO could be essentially limited by the edge value $n_0 \sim 0.35\,n_{\mathrm{G}}$, which we will prove to have a more fundamental MHD origin (see sections 3, 4).

3. Role of thermal instabilities

3.1. The MARFE in FTU and RFX

An important point to raise is the role of the thermal instabilities in setting the environment for the development of the density

limit. In both RFX and FTU, the density limit is associated with the appearance of the multifaceted asymmetric radiation from the edge (MARFE) [40, 41]. In FTU, the MARFE is an annulus of radiative-unstable plasma, which appears at $n_0 > 0.4\,n_G$ [31] as a toroidal ring, poloidally localized, as shown in figure 3(*a*). The threshold $0.4\,n_G$ is consistent with the Lispschultz scaling of the MARFE critical density with $I_p/\pi a^2$ [40]. This toroidal MARFE is caused by a reduction of parallel electron conductivity, which prevents the energy from redistributing along the flux surface, and lets the formation of local cold regions with strong line emission, in the high field side, where the heat flux from the core is lower [42]. In TEXTOR, Tokar' provided a nice, simple model of this phenomenon, interpreted as a local imbalance between parallel heat diffusion and ionization/radial particle transport [43]. In that model, the critical density scales as

$$n_0^{(cr)} = \frac{1}{q_a}\sqrt{\frac{\kappa_\parallel a}{60\pi R^2 D_\perp \sigma_{ion}}}, \qquad (4)$$

$\kappa_\parallel$ being the parallel heat diffusivity, $D_\perp$ the cross-field particle diffusivity, and σ_{ion} the cross-section for the ionization process. This scaling is consistent with the scaling found in FTU.

Contemporary with the MARFE, in FTU a 2/1 mode starts in the high density regime during the density ramp-up and grows up to high amplitude in the final phase of discharge preceding the density limit disruption [44]. The mode onset is in agreement with linear stability calculations, confirming that its appearance is correlated with a peaking of the current profile associated to the cooling of the edge plasma, as we will discuss in detail in section 4.

In the RFP, the MARFE appears at $n_0/n_G > 0.5$ as a poloidal ring of high radiation, toroidally localized, as shown in figure 3(*b*). Radiation comes from He-like impurity lines (mainly O and C) excited by low temperatures in the annulus: there is no evidence of strong recombination, as deduced from the behaviour of the ratio of the H_γ/H_α lines along the toroidal angle [20].

The unusual symmetry of the RFP MARFE is easily explained, taking into account that the equilibrium field is toroidal in the FTU edge, poloidal in the RFP edge. Rather than being a simple problem of energy redistribution (as it is the case with the Tokar' model), the MARFE in RFX is instead linked with a well-defined $\vec{E}\times\vec{B}$ flow pattern. The trigger of the MARFE mechanism in the RFP is the 0/1 island, which resonates at $q = 0$ in the RFP edge [45] and it is destabilized at $n_0/n_G \sim 0.35$, as already mentioned in section 2.1. This island grows with n/n_G, as shown in figure 4: frame (*a*) reproposes the explosive growth of the 0/1 mode at $I_p = 800$ kA, already discussed in figure 1(*b*); frames (*b*)–(*d*) show a Poincaré plot of the island, in three discharges with increasing n/n_G, corresponding to the coloured circles in figure 4(*a*). Islands are plotted using as input the eigenfunctions calculated by the code NCT in toroidal geometry [46]: the radial width of the island is largely determined by the value of $B^r_{0,1}$ at $r = a$ [47]. The island grows to a critical size at $n_0/n_G \approx 0.5$, when it touches the wall (figure 4(*d*)): this is a necessary condition for driving electron transport along the magnetic field in regions of very short connection length L_c, as already discussed in the past on RFX [26, 48] and TEXTOR [49–51] edge stochastic layers. We can estimate the critical amplitude of the island as $B^r_{0,1}/B_{\theta,a} \sim 0.1\%$, which corresponds to $B^r_{0,1} \approx 3$ gauss at $I_p = 800$ kA and $q_a = -0.015$. The critical size of the island depends on q_a: with lower (more negative) $q_a = -0.03$ (reversal parameter $F = -0.2$), the critical amplitude for wall wetting almost doubles, with $B^r_{0,1} \approx 6$ G (normalized value 0.3%), as reported in a previous work [21], since the resonance is moved further inside the plasma. Despite this, the threshold in n/n_G remains unchanged, because $m = 0$ modes are destabilized at lower q_a [29], so that the initial size of the 0/1 island is also larger. In this sense, the threshold in n/n_G is the result of a competing process between island width and wall proximity, as pointed out in [48].

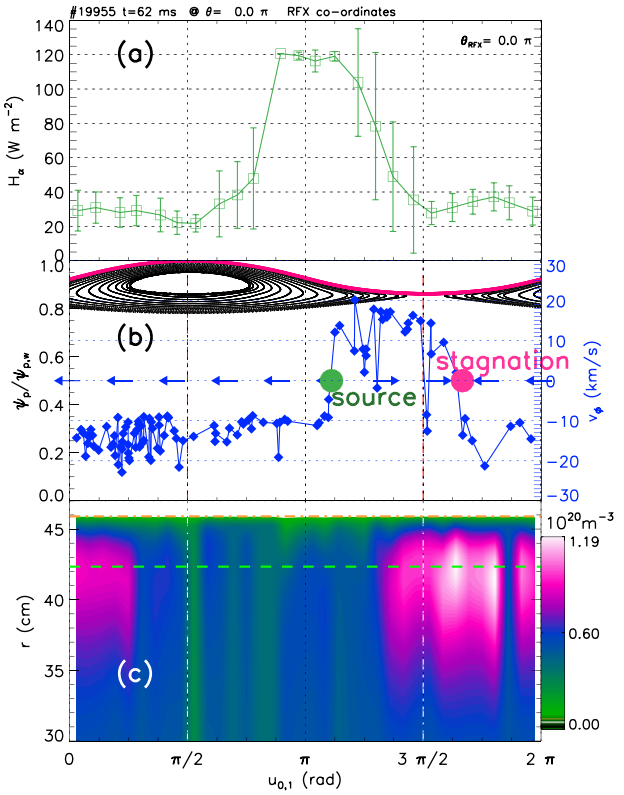

Figure 5. Example of MARFE in the RFX RFP. (*a*) H_α emissivity (green) as a function of the helical angle $u_{0,1}$; (*b*) the 0/1 island (black) and the plasma flow v_φ (blue). The convective cell is highlighted by arrows, with the source and stagnation points; (*c*) electron density map.

In summary, this paper strongly supports the idea that edge islands are a fundamental aspect in the Greenwald phenomenon: it is curious to notice that a similar behaviour for the 2/1 island in the tokamak, follows from a 3D generalization of the Rutherford equation with an explosive radiative term [52]. In the RFP, experiments show that the threshold for 0/1 destabilization is slightly smaller with strong Neon puffing ($n_0/n_G \sim 0.3$), but impurities seem not to be a fundamental ingredient in the island growth process.

3.2. Plasma flow and MARFE

The growth of the 0/1 island is associated with a pathological behaviour of the toroidal component of the plasma flow v_φ,

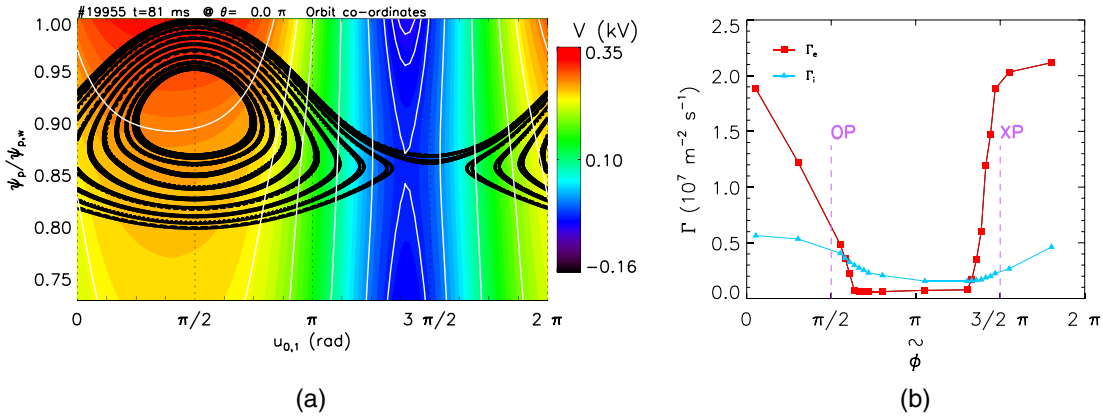

Figure 6. Simulation of a convective cell in the RFP, with the code Orbit. (*a*) Plot of the (0, 1) island (black line), along with a contour plot of the ambipolar potential required to ensure quasi-neutrality in the edge plasma: colours correspond to the values of the potential, in kV. Contour levels of Φ (in white) highlight the topology of the potential, with a saddle corresponding to $u \sim 3/2\pi$. This saddle structure corresponds to the measured convective cell of figure 5; (*b*) electron and ion fluxes as a function of the potential phase $\tilde{\phi}$.

which in the RFP corresponds to the $\vec{E} \times \vec{B}$ flow ($v_\varphi \approx E_r/B_\theta$). The flow v_φ is generally negative along the toroidal angle [21]. When the island grows to the critical size shown in figure 4(*d*), v_φ reverses direction, with the formation of two null points, source and stagnation, as shown in figure 5(*b*). A similar reversal of the perpendicular flow is seen also in the C-mod tokamak when $n_0/n_G \gtrsim 0.35$ [9, 10], and, more recently, also on ASDEX at a comparable normalized density [12]. A crucial point of the flow analysis in RFX was to map the toroidal angle into the helical angle of the perturbation [53]: in the 0/1 case it is trivially $u_{m,n} = m\theta - n\varphi + \phi = -\varphi + \phi$ (ϕ phase of the mode). In this way, one can clearly recognize the presence of a source and a stagnation point, with the latter corresponding to the toroidally localized MARFE, as shown in figure 5(*b*). The *source* corresponds instead to the maximum H_α signal, which stands in between the O-point (OP) and X-point(XP) of the main island, at $u \approx \pi$ (figure 5(*a*)). In fact, it is a well-known result in the RFP that the phase-locking of the $m = 1$ TMs at $u = \pi$ (i.e. shifted 90° toroidally from the OP of the 0/1 island) is a preferential source of particles and localized PWI [54].

On the contrary, the *stagnation point* corresponds to the XP of the 0/1 island, at $u \sim 3/2\pi$: here the density radial profile becomes markedly hollow, with an edge-localized peak as large as $\sim 1.5\, n_G$, as shown in figure 5(*c*). The cold and overdense plasma in the region of the XP is ultimately responsible for the radiative behaviour and the MARFE, as shown in figure 3(*b*). The connection between MARFE and $m = 0$ islands is confirmed by recent RFX experiments, where by removing the $q = 0$ resonance, edge density peaking is avoided [55]. It is also consistent with experiments done in TEXTOR, where the critical density for the MARFE onset was seen to decrease with the amplitude of static, edge islands produced via resonant magnetic perturbations (RMPs): the larger the island, the sooner the MARFE would appear [56].

Our interpretation of the MARFE as due to an $\vec{E} \times \vec{B}$ convective cell is radically different from the traditional model of equation (4): in fact, while in the traditional approach the critical density is set by the ratio $\sqrt{\kappa_\parallel/D_\perp}$ (parallel heat transport to perpendicular diffusivity), in the RFP we have shown that a new, critical element is the ratio between the two perpendicular transport terms, radial diffusion and toroidal convection, $D_r/v_\varphi L_n$ (with L_n the density gradient characteristic length). The convective term $v_\varphi L_n$ in the RFP can be two orders of magnitude larger than the diffusive term, as it has been shown elsewhere [21]. In RFX low current discharges, it is possible to measure also the radial component of the flow, v_r, with insertable probes (even if in a different symmetry, the helical 1/7), thus confirming the presence of a *convective cell*, dragging plasma along the helical angle [57, 58]. $\vec{E} \times \vec{B}$ convective cells have been measured around edge-resonant islands in tokamaks and stellarators [59–62] and provide an interesting link between the density limit and experiments with RMPs. In this sense, the density limit can be seen as a *particular instance* of the more general problem of the plasma response to RMPs.

3.3. Modelling of the convective cell

In the RFP, the convective cell has been modelled with the guiding-centre code Orbit [63], showing that the 0/1 flow pattern corresponds to an ambipolar potential, balancing electron radial diffusion between the OP and XP of the island, which is embedded in the RFP stochastic edge [64]. In fact, the connection length L_c is larger, by more than 3 orders of magnitude, at the XP, with respect to the OP: in classical mechanics, orbits (=magnetic field lines) take infinite 'time' (i.e. infinite parallel length) to perform a complete excursion around the XP along the separatrix. These long excursions take the name of 'homoclinic tangles', and are commonly found e.g. in diverted tokamaks [65]. Electrons, having a smaller Larmor radius, are more sensitive to the resonant tangle present around the XP [21]: ions instead average out the toroidal asymmetry of L_c. This causes a small charge imbalance [66] (order $10^{13} \div 10^{14}\,\mathrm{m}^{-3}$) along u, which is immediately counteracted by an electrostatic potential with the same symmetry as the 'parent' island. This is shown in figure 6(*a*), where the 0/1 island is over-plotted to the contour map of the ambipolar potential: by definition, the flow is such that $\vec{v} \cdot \nabla\Phi = 0$, so the saddle point in the contour

corresponds to the measured, convective cell. ORBIT predicts a correct amplitude, phase and geometry of the potential, with the potential well (positive bulge of v_φ) staying in proximity of the XP of the island, as it is evident by comparing figure 6(a) with figure 5(b). Moreover, if one searches for an algebraic solution to the ambipolar constraint $\Gamma_e = \Gamma_i$ as a function of the potential phase $\tilde{\phi}$, one can find a second root, in addition to the known solution at the XP. This second root has the potential well at the OP (see figure 6(b)). The presence of two roots, instead of a single one as previously found [64], is a recent result which has been obtained after modifying ORBIT guiding centre equations [63] to correctly express electron drifts. Interestingly enough, recent simulations of the 4/1 islands generated with a RMP in TEXTOR, show a similar behaviour of the connection length L_c [51, 64], and also the presence of two roots for the model of ambipolar potential, one with the potential well at the OP, the other at the XP [67]. The solution matching TEXTOR experimental data is stable in the thermodynamic sense usually followed for stellarators [68], that opens interesting possibilities also for the RFX case: it shows that in principle it is possible, by acting on the T_e/T_i ratio, to make the system flip from one root to the other, e.g. with additional heating of the electron/ion channel (ECRH or ICRH). This is an interesting extension of the theory of ambipolar roots in the stellarator, applied to edge stochastic layers. Indeed, compelling experimental evidence in FTU with ECRH targeted on the 2/1 island will be shown in section 4.

As a final remark, it is worth recalling that the presence of an XP, namely, of a resonance generated e.g. via magnetic field reconnection, seems to be a necessary condition for the reversal of the perpendicular component of the flow: a simple edge ripple is not sufficient to reverse the flow, as observed in the case of a 1/7 mode in RFX-mod, which resonates well inside the plasma [48, 53, 58, 66]. In fact, a ripple of the toroidal flux ψ along φ can be canonically transformed in a constant helical flux χ along the helical angle u [47]: electrons, as a first approximation, follow the helical flux χ, and thus only a simple modulation of density and temperature along φ is seen.

The role of edge islands in the stellarator (a.k.a. 'low-order' rationals) has been studied in relationship with turbulence: it has been reported that configurations with $\iota = 1/q$ close to rational values experience more easily confinement transitions to the H-mode, accompanied by a strong reduction of broadband turbulence [69]. The connection between these islands and radiation-driven collapses has not been investigated in detail, although edge islands could play a role by increasing edge temperature [70].

4. Destabilization of MHD modes

Having established in the RFP a connection between MARFE, islands and E^r, it is interesting to explore this possibility in the tokamak. High-density disruptions in FTU are always preceded by a strong 2/1 MHD activity [44], as already noted by Granetz in the 1980s [3]. A comparison study on this point can be done in both machines, FTU and RFX, run in tokamak configuration. An example of a RFX-mod tokamak discharge near the density limit is shown in figure 7. The critical density

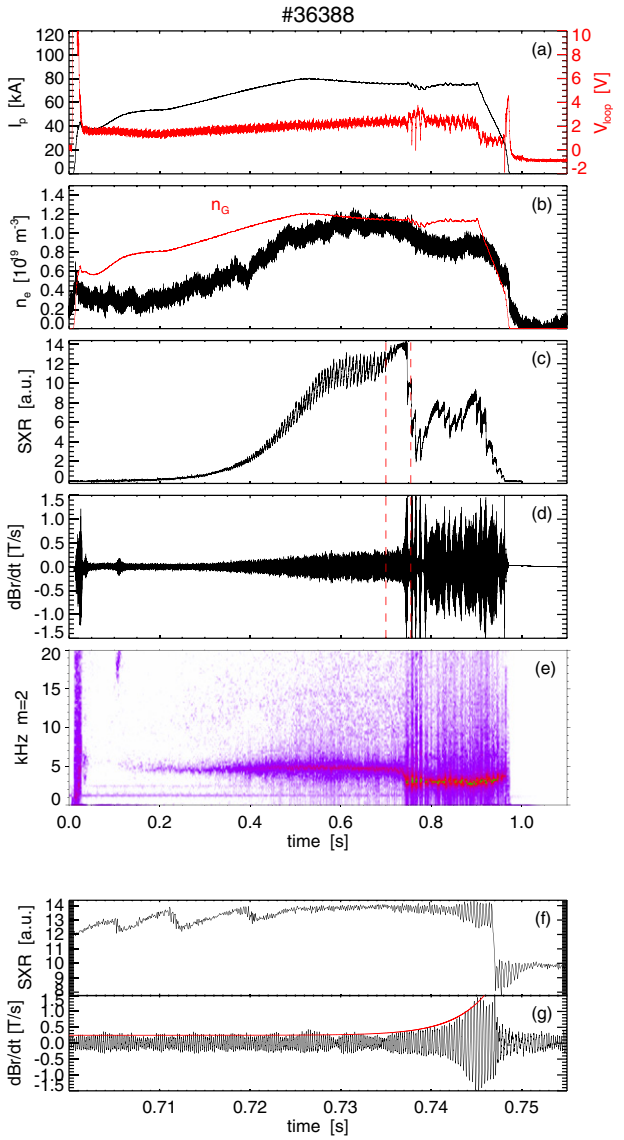

Figure 7. Example of disruption in the RFX experiment, run in tokamak configuration. Time evolution of (a) plasma current and loop voltage, (b) density (black) and Greenwald parameter (red), (c) central SXR emission, (d) $\dot{B}_r$ signal, with in-vessel pick-up probes, (e) spectrogram of the 2/1 component. Panels (f) and (g) are the expanded inset in between the vertical, dashed lines of (c) and (d), respectively: they show the final stage of the disruption (f), when the 2/1 mode grows exponentially (g).

condition is associated with a rapid variation of the rotating 2/1 TM, which, as shown in the spectrogram of figures 7(d)–(e), rapidly reduces its frequency and exponentially grows on a characteristic time scale of ∼3 ms . The final phase, with the exponential increase, is marked by the dashed, vertical lines in (c)–(d), and it is expanded in figures 7(f)–(g). It is interesting to note that in RFX-mod such MHD activity induces a thermal quench in the plasma, as deduced by the rapid collapse of the SXR signal (figure 7(c)), but not necessarily a current quench (figure 7(a)): hence, only a minor disruption is observed. In the RFX-mod we explored a range of $q_a = 1.6 \div 4.6$, in order to investigate the role of the 2/1 resonance inside the plasma. In discharges with $q_a < 2$, along with an increased

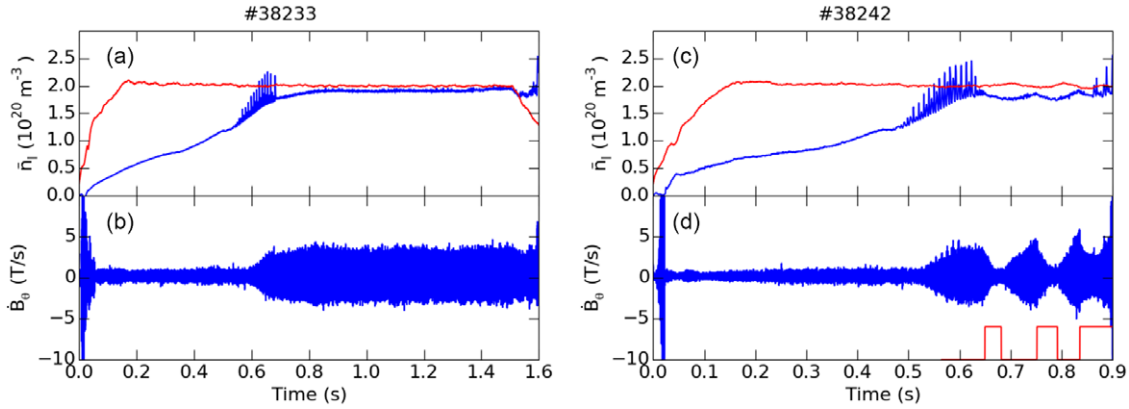

Figure 8. Example of stabilization of the 2/1 mode in the FTU tokamak at high density. (*a*) Line-averaged electron density $\bar{n}_e$ (in blue), and Greenwald parameter n_G (in red) for a standard FTU discharge near the density limit. $n_0 \sim n_G$ at the end of the ramp; (*b*) $\dot{B}_\theta$ signal, for the same discharge as in (*a*); (*c*) density and Greenwald parameter for the same type of discharge, but with ECRH targeted on the 2/1 resonance; (*d*) $\dot{B}_\theta$ signal, with ECRH injection. Red bars in (*d*) indicate the ECRH phase.

broadband MHD activity, it has been found that the 2/1 mode is superseded by the 3/2 mode, resonant close to the edge, exhibiting almost the same growth and locking properties. Finally, it is worth mentioning that the 2/1 mode modulates the radial electric field E^r at the edge, with a clear $m = 2$ periodicity [58].

Also in FTU a strong 2/1 activity is seen in the high density regime. The TM starts during the density ramp-up. Initially, the mode grows algebraically and its frequency remains constant. Subsequently, the mode growth speeds up and the frequency decreases to zero. The analysis of the linear stability of this classical TM has shown a destabilization with increasing peaking of the current profile during the density ramp-up, confirming the usual explanation for the appearance of a low-order TM when density increases [44]. Experiments of real time control of TM instability using injection of electron cyclotron waves (ECRH) inside the magnetic island have been recently performed on FTU [71], on the wake of results of disruption healing obtained in the past on FTU [72] and ASDEX [73]. The novelty is that here we consider discharges near the density limit, in which a 2/1 TM has been induced by a density ramp. The reference discharge is shown in figure 8(*a*): in this discharge, $q_a = 5$, so that at the end of the density ramp (shown by the blue line) the B-limit and the Greenwald limit coincide, with $n_0 \approx n_G$ (red line = Greenwald parameter). At the end of the ramp, the 2/1 mode onset is evident from the signal of $\dot{B}_\theta$ (figure 8(*b*)). Based on this scenario, a real-time control system is used, where the trigger given as input to the feedback algorithm is an MHD instability marker. This marker uses a 3D array of pick up coils [74], where a low value indicates that the 2/1 island is present. One gyrotron beam of 0.4 MW, 140 GHz, max pulse duration of 0.5 s is used for heating, with the EC absorption radius defined by means of a statistical scaling obtained for the mode radius in the high density regime. The controlled discharge is shown in figure 8(*c*). A complete suppression of the MHD amplitude has been obtained during the ECRH phase, as it is evident in the $\dot{B}_\theta$ signal shown in figure 8(*d*). Nevertheless, in some cases, after a prolonged heating, the instability newly starts to increase, probably due to a radial shift of the resonance (see figure 8(*d*) at $t \sim 0.9$ s). These results are quite relevant, if interpreted in the light of the simulations with Orbit, where the ambipolar potential depends on the T_e/T_i ratio [68]: in this way, ECRH, locally modifying the T_e/T_i ratio at the 2/1 resonance, could make the system flip from one ambipolar solution to the other (figure 6(*b*)), thus modifying the whole pattern of E^r. Unfortunately, no direct measurements of E^r on conjunction with ECRH are presently available in FTU: these are planned for years 2015–16.

5. Conclusion

We have shown new data coming from the FTU tokamak, and RFX-mod run as tokamak and reversed-field pinch (RFP), supporting a new interpretation of the Greenwald density limit as due to a critical MHD condition in the edge plasma. In both tokamak and RFP an edge density critical value $n_{edge} \sim 0.35 n_G$ has been found: the central density follows instead a scaling with the magnetic field, $n_0 \propto B^{1.5}$. The double nature of the density limit, with an edge Greenwald scaling and a core B-scaling, was indeed present in the early research on this subject, and should be considered in the design for DEMO.

The edge limit has been extensively studied in the RFP, where it has been shown to be strictly related to an $\vec{E} \times \vec{B}$ convective cell (and associated MARFE formation) caused by an edge resonating island. The convective cell arises as an ambipolar response of the plasma to the presence of the island fixed points, and has been successfully simulated via the guiding centre code Orbit. Convective cells are also measured around edge islands created with resonant magnetic perturbations (RMPs). In this way, the edge density limit can be seen as a particular instance of the more general problem of the plasma response to 3D perturbations. In any case, this edge MHD limit can be crossed in the RFP without causing a disruption: the maximum achievable density in the RFP is proportional to the heating power, $n_0 \propto P_{ohm}$, similarly to the Sudo scaling in the stellarator.

Also in FTU a 2/1 tearing mode is destabilized at high density, even if the link with the MARFE is not as clear as in

the RFP. The 2/1 mode can be stabilized with ECRH, targeted on the 2/1 resonance, which is consistent with the interaction of the electron heating with an ambipolar mechanism governed by the T_e/T_i ratio. This provides a viable tool for overcoming the Greenwald limit in the edge plasma.

Acknowledgments

The authors would like to thank Dr David Terranova for calculating the toroidal equilibrium in the NCT code, and Dr Samuele Dal Bello, chief engineer in charge of the RFX-mod machine operation. This work has received funding from the European Union's Horizon 2020 research and innovation programme under grant agreement number 633053 as Enabling Research Project CfP-WP14-ER-01/ENEA_RFX-01.

References

[1] Greenwald M. *et al* 1988 *Nucl Fusion* **28** 2199
[2] Hugill J. *et al* 1979 *Proc. 9th European Conf. on Controlled Fusion and Plasma Physics (Petit Lancy, Switzerland, 1979)* vol 1 (Oxford: European Physical Society) p 151
[3] Granetz R.S. 1982 *Phys. Rev. Lett.* **49** 658–61
[4] Sudo S. *et al* 1990 *Nucl. Fusion* **30** 11
[5] Zohm H. *et al* 2013 *Nucl. Fusion* **53** 073019
[6] Mertens V. *et al* 1997 *Nucl. Fusion* **37** 1607
[7] Mertens V., Borrass K., Gafert J., Laux M., Schweinzer J. and the ASDEX Upgrade Team 2000 *Nucl. Fusion* **40** 1839–43
[8] Borrass K. *et al* 2004 *Nucl. Fusion* **44** 752–60
[9] Agostini M., Terry J., Scarin P. and Zweben S. 2011 *Nucl. Fusion* **51** 053020
[10] Cziegler I., Terry J.L., Hughes J.W. and LaBombard B. 2010 *Phys. Plasmas* **17** 056120
[11] Antar G.Y., Counsell G. and Ahn J.W. 2005 *Phys. Plasmas* **12** 082503
[12] Carralero D. *et al* 2014 *Nucl. Fusion* **54** 123005
[13] Scarin P. *et al* 2007 *J. Nucl. Mater.* **363–65** 669–73
[14] Ortolani S. and the RFX Team 2006 *Plasma Phys. Control. Fusion* **48** B371
[15] Bolzonella T. *et al* 1999 *Proc. 26th EPS Conf. on Plasma Physics (Petit Lancy, Switzerland, 1999)* vol 23J ed R.M. Pick *et al* (Maastricht: European Physical Society) pp 1169–72 http://epsppd.epfl.ch/Maas/web/pdf/p3057.pdf
[16] Bartiromo R. *et al* 2000 *Proc. 27th EPS Conf. on Plasma Physics (Petit Lancy, Switzerland)* vol 24B ed K. Szegö *et al* (Budapest: European Physical Society) pp 1380–3 http://epsppd.epfl.ch/Buda/pdf/p4_031.pdf
[17] Valisa M. and the RFX Team 2004 *Proc. 20th Int. Conf. on Fusion Energy 2004 (Vilamoura, Portugal, 2004)* (Vienna: IAEA) pp CD–ROM file EX/P4–13 www-naweb.iaea.org/napc/physics/fec/fec2004/papers/ex_p4-13.pdf
[18] Valisa M. *et al* 2006 *Proc. 21st Int. Conf. on Fusion Energy (Chengdu, People's Republic of China, 10–21 October 2006)* (Vienna: IAEA) pp CD–ROM file EX/P3–17 www-naweb.iaea.org/napc/physics/FEC/FEC2006/papers/ex_p3-17.pdf
[19] Puiatti M.E. *et al* 2009 *Phys. Plasmas* **16** 012505
[20] Puiatti M.E. *et al* 2009 *Nucl. Fusion* **49** 045012
[21] Spizzo G. *et al* 2010 *Plasma Phys. Control. Fusion* **52** 095011
[22] Carraro L., Innocente P., Puiatti M.E., Sattin F., Scarin P. and Valisa M. 1995 *Proc. 22nd EPS Conf. on Plasma Physics (Petit Lancy, Switzerland, 1995)* vol 19C ed B.E. Keen *et al* (Bournemouth: European Physical Society) pp 161–4
[23] Puiatti M. *et al* 2013 *Nucl. Fusion* **53** 073001
[24] de Vries P.C., Rapp J., Schüller F.C. and Tokar' M.G. 1998 *Phys. Rev. Lett.* **80** 3519–22
[25] Wyman M. *et al* 2009 *Nucl. Fusion* **49** 015003
[26] Spizzo G. *et al* 2012 *Nucl. Fusion* **52** 054015
[27] Marrelli L. *et al* 2007 *Plasma Phys. Control. Fusion* **49** B359–69
[28] Puiatti M.E. *et al* 2013 *Plasma Phys. Control. Fusion* **55** 124013
[29] Cappello S. 2004 *Plasma Phys. Control. Fusion* **46** B313–25
[30] Gormezano C., Di Marco F., Mazzitelli G., Pizzuto A., Righetti G., Romanelli F. and the FTU Team 2004 *Fusion Sci. Technol.* **45** 297–302 http://epubs.ans.org/?a=515
[31] Pucella G. *et al* 2013 *Nucl. Fusion* **53** 023007
[32] Pucella G. *et al* 2013 *Nucl. Fusion* **53** 083002
[33] Isichenko M.B., Gruzinov A.V. and Diamond P.H. 1995 *Phys. Rev. Lett.* **74** 4436–9
[34] Romanelli M. *et al* 2007 *Plasma Phys. Control. Fusion* **49** 935
[35] Murakami M., Callen J. and Berry L. 1976 *Nucl. Fusion* **16** 347
[36] Piovesan P. *et al* 2013 *Phys. Plasmas* **20** 056112
[37] Carati A., Zuin M., Maiocchi A., Marino M., Martines E. and Galgani L. 2012 *Chaos* **22** 033124
[38] Bell M. *et al* 1992 *Nucl. Fusion* **32** 1585
[39] Lang P. *et al* 2014 *Nucl. Fusion* **54** 083009
[40] Lipschultz B. 1987 *J. Nucl. Mater.* **145–147** 15–25
[41] Samm U. *et al* 1999 *J. Nucl. Mater.* **266–269** 666–672
[42] Tudisco O. *et al* 2010 *Fusion Eng. Des.* **85** 902–9
[43] Tokar M.Z. *et al* 1999 *J. Nucl. Mater.* **266–269** 958–62
[44] Pucella G., Botrugno A., Buratti P., Giovannozzi E., Marinucci M., Tudisco O. and the FTU Team 2013 *Proc. 40th EPS Conf. on Plasma Physics (Petit Lancy, Switzerland, 2013)* vol 37D ed V Naulin *et al* (Helsinki: European Physical Society) p P5.139 http://ocs.ciemat.es/EPS2013PAP/pdf/ P5.139.pdf
[45] Spizzo G. *et al* 2006 *Phys. Rev. Lett.* **96** 025001
[46] Zanca P. and Terranova D. 2004 *Plasma Phys. Control. Fusion* **46** 1115
[47] Ciaccio G., Veranda M., Bonfiglio D., Cappello S., Spizzo G., Chacon L. and White R.B. 2013 *Phys. Plasmas* **20** 062505
[48] Scarin P. *et al* 2011 *Nucl. Fusion* **51** 073002
[49] Schmitz O. *et al.* 2009 *J. Nucl. Mater.* **390–391** 330–4
[50] Stoschus H. *et al* 2012 *Nucl. Fusion* **52** 083002
[51] Ciaccio G. *et al* 2014 *Nucl. Fusion* **54** 064008
[52] White R.B., Gates D. and Brennan D. 2015 Explosive island destabilization and the Greenwald limit *Phys. Plasmas* **22** 022514
[53] Vianello N. *et al* 2013 *Nucl. Fusion* **53** 073025
[54] Marrelli L., Zanca P., Martin P., Martini S. and Murari A. 1999 *J. Nucl. Mater.* **266–269** 877–883
[55] De Masi G., Auriemma F., Cavazzana R., Martines E. and Spizzo G. 2014 *Bull. Am. Phys. Soc.* **59** 256
[56] Liang Y. *et al* 2005 *Phys. Rev. Lett.* **94** 105003
[57] De Masi G. *et al* 2013 *Nucl. Fusion* **53** 083026
[58] Vianello N. *et al* 2015 *Plasma Phys. Control. Fusion* **57** 014027
[59] Evans T.E. *et al.* 1987 *Proc. 14th EPS Conf. on Plasma Physics (Petit Lancy, Switzerland, 1987)* vol 11D ed F. Engelmann and J.L. Alvarez Rivas (Madrid: European Physical Society) pp 770–3
[60] McCool S. *et al* 1990 *Nucl. Fusion* **30** 167
[61] Takamura S., Ohnishi N., Yamada H. and Okuda T. 1987 *Phys. Fluids* **30** 144–7
[62] Ida K. *et al* 2004 *Nucl. Fusion* **44** 290
[63] White R.B. and Chance M.S. 1984 *Phys. Fluids* **27** 2455–67
[64] Spizzo G. *et al* 2014 *Phys. Plasmas* **21** 056102
[65] Evans T.E., Roeder R.K.W., Carter J.A. and Rapoport B.I. 2004 *Contrib. Plasma Phys.* **44** 235–40
[66] Scarin P. *et al* 2013 *J. Nucl. Mater.* **438** (Suppl.) S550–3

[67] Ciaccio G. *et al* 2015 Helical modulation of the electrostatic potential due to magnetic islands in toroidal plasma confinement devices *Nucl. Fusion* submitted
[68] Hastings D., Houlberg W. and Shaing K. 1985 *Nucl. Fusion* **25** 445
[69] Estrada T. *et al* 2009 *Plasma Phys. Control. Fusion* **51** 124015
[70] Tabarés F.L. *et al* 2008 *Plasma Phys. Control. Fusion* **50** 124051
[71] Sozzi C. *et al* 2014 *Proc. 25th Int. Conf. on Fusion Energy (St Petersburg, Russian Federation, 13–18 October 2014)* (Vienna: IAEA) pp CD–ROM file EX/P2–47
[72] Esposito B. *et al* 2008 *Phys. Rev. Lett.* **100** 045006
[73] Esposito B. *et al* 2009 *Nucl. Fusion* **49** 065014
[74] Galperti C. *et al* 2014 *Plasma Phys. Control. Fusion* **56** 114012